Journal of Magnetism and Magnetic Materials 322 (2010) 1784–1792

Contents lists available at ScienceDirect

Journal of Magnetism and Magnetic Materials

journal homepage: www.elsevier.com/locate/jmmm

Nanocrystals and amorphous matrix phase studies of Finemet-like alloys containing Ge

J.A. Moya [a,b,c,*]

[a] IESIING, Facultad de Ingeniería e Informática, UCASAL, A4402FYP Salta, Argentina
[b] Lab. Sólidos Amorfos, Facultad de Ingeniería, INTECIN, UBA-CONICET, Argentina
[c] CONICET, Argentina

ARTICLE INFO

Article history:
Received 17 November 2009
Available online 23 December 2009

Keywords:
Nanocrystalline material
Soft magnetic material
Mössbauer spectroscopy
Amorphous material

ABSTRACT

Two simple models were developed in order to determine the chemical composition of both nanocrystals and intergranular amorphous phases in nanocrystallized $Fe_{73.5}Si_{13.5}B_9Nb_3Cu_1$ containing Ge using data from X-ray diffraction and Mössbauer spectroscopy techniques. Saturation magnetization of the amorphous intergranular matrix (M_s^{am}) was calculated considering the contribution of the α-Fe(Si,Ge) nanocrystals and saturation magnetization of the alloys. The behavior of M_s^{am} with the iron content of the matrix was obtained and discussed. The exchange stiffness constant for the nanograins and for the amorphous phases was determined. The increment in the coercive field (H_c) with increasing Ge content was evaluated using two theoretical models for the random magnetocrystalline anisotropy constant ($\langle K_1 \rangle$). Results show that the magnetic hardening observed could not be attributed to an increase in $\langle K_1 \rangle$ but mainly to an important increment of the magnetostriction constant of the α-Fe(Si,Ge) nanocrystals (λ_s^{cr}). Values for λ_s^{cr} are proposed.

1. Introduction

Since their discovery [1], soft magnetic nanocrystalline alloys have raised great interest because of their excellent soft magnetic properties: while maintaining a low coercive field ($H_c \sim 1$ A/m) and very high susceptibility ($\mu_i = 10^5$, at 1 kHz) their saturation magnetization is high ($M_s = 1.3$ T) and the magnetostriction remains relatively small ($\lambda_s \sim 10^{-6}$).

The main factors for this are the spatial distribution and the relative quantity of the nanograins in the amorphous matrix. (i) The matrix is an amorphous ferromagnet with a reduced magnetocrystalline anisotropy: the exchange interaction length, which is greater than the structural correlation length (grain size), controls the magnetization process and consequently, the macroscopic magnetocrystalline anisotropy is averaged out [2]. (ii) Crystals of 10–20 nm grain diameter constitute the crystalline phase conferring a higher M_s to the material. Its magnetocrystalline anisotropy is at least three times greater than that of the amorphous matrix but also results averaged out when these nanograins are immersed in a ferromagnetic amorphous matrix. (iii) Furthermore, in the case of FINEMET-like alloys, the effective magnetostriction constant of the whole material is reduced about one order of magnitude because of the compensation effect between the negative magnetostriction of the α-Fe(Si) phase ($\lambda_s = -6 \times 10^{-6}$) and the positive value of the amorphous one ($\lambda_s = 22 \times 10^{-6}$) [3,4].

Herzer [5,6] was the first to explain the soft magnetic properties of nanocrystalline materials in terms of the random magnetocrystalline anisotropy model ($\langle K_1 \rangle$), considering them a single-phase system: $\langle K_1 \rangle = v^{cr2} K_1^4 D^6 / A_{cr}^3$ where v^{cr} is the crystalline volume fraction, D the grain diameter and A_{cr} the exchange stiffness constant of the crystalline phase. Lately, Hernando et al.[7] and Suzuki and Cadogan [8] independently introduced the two-phase nature of nanocrystalline materials in Herzer's model. Suzuki and Cadogan, in particular, established the dependence on $\langle K_1 \rangle$ also from the exchange stiffness constant of the amorphous phase (A_{am}).

There is a lot of research on the addition of diverse elements into the FINEMET composition (see for example reviews on Refs. [9,10]). The effect on the crystalline phase can be related not only to each one of the parameters affecting $\langle K_1 \rangle$ (i.e., grain diameter, magnetocrystalline anisotropy, exchange stiffness constant and crystalline volume fraction), but also to magnetoelastic anisotropy via magnetostriction changes. Chemical and volume fraction changes in the crystalline phase will affect chemical composition of the amorphous matrix and, hence, its exchange stiffness and λ_s constants. The present work makes a review of

* Correspondence address: IESIING, Facultad de Ingeniería e Informática, UCASAL, A4402FYP Salta, Argentina. Tel.: +54 387 4268939.
E-mail address: jmoya.fi.uba@gmail.com

0304-8853/$ - see front matter © 2009 Elsevier B.V. All rights reserved.
doi:10.1016/j.jmmm.2009.12.030

prvious reports [11–14] that investigate the effect of the addition of Ge in nanocrystallized alloys. Here, a new data analysis is performed to calculate nanocrystal chemical compositions (Section 4.1), volume fraction of crystalline and amorphous phases (Section 4.2), amorphous matrix composition (Section 4.3) and saturation magnetization and exchange stiffness of crystalline and amorphous phases (Section 4.4). Finally, Herzer and Suzuki's models are used in order to determine the origin of the magnetic hardening that occurs when Ge is added to the FINEMET composition (Section 4.5). As a result, values for the magnetostriction constant of the α-Fe(Ge,Si) crystals are proposed.

2. Experiment

We used the melt spinning technique to obtain amorphous FINEMET-type ribbons with different Ge content. The following samples were produced (chemical composition in at%): (i) series A samples $Fe_{73.5}Si_{13.5-x}Ge_xNb_3B_9Cu_1$ (x=0, 7, 8, 10, 13.5) namely Ge0, Ge7, Ge8, Ge10 and Ge13.5, respectively [11,15], (ii) samples Ge6* with $Fe_{71.5}Si_{9.5}Ge_6B_9Nb_3Cu_1$ and (iii) sample Ge15.5* with $Fe_{73.5}Ge_{15.5}Nb_3B_7Cu_1$[14]. Samples were submitted to a heat treatment at different temperatures for 1 h in order to induce nanocrystallization; the samples analyzed here correspond to annealing temperature conditions with optimum soft magnetic properties, i.e., 540 °C for series A and Ge6* samples and 550 °C for sample Ge15.5*.

X-ray diffraction (XRD) was performed with a Rigaku diffractometer with monochromatized Cu Kα radiation. Mössbauer spectroscopy (MS) was carried out in transmission geometry using a ^{57}Co in Rh source. The fitting procedure of Mössbauer spectra in this kind of materials is a matter of continuous discussion regarding the number of subspectra corresponding to the crystalline sites (from 4 to 7) and the function for fitting the area corresponding to the amorphous phase. The amorphous phase has a large distribution of hyperfine parameters and usually is observed as bimodal: it is not clear whether this is due to the presence of two distinct iron concentration regions [16] or to some effect of the electric quadrupole interaction at low magnetic hyperfine fields [17]. The distribution can be fitted with Gaussian or discrete distributions, or large sextets with Lorenzian, Gaussian or pseudo-Voigt line shapes. For a review see Refs. [18,19] and references therein. From a good quality fit, we can obtain accurate information about the quantity of amorphous and crystalline phases and their chemical composition.

In previous work [11], we used the DIST and SITE versions of the NORMOS program [38] to fit the spectra. Our DIST version allows combining distributed hyperfine magnetic parameters (useful for amorphous phases) with up to five crystalline subspectra, while the SITE version only allows fitting discrete subspectra. Both versions were used to evaluate the amorphous phase in partially nanocrystallized samples: SITE with two wide sextets, and DIST with two Gaussian distributions with a linear dependence of the hyperfine magnetic field (Bhf) on the isomer shift (IS). Comparison between both kinds of fittings did not show significant differences in the hyperfine parameters of samples annealed at 540 °C. Hence, we report here the results obtained using the SITE program that allows employing six sextets ($S1$–$S6$) to analyze the nanocrystalline phases and two wide sextets for fitting the subspectra corresponding to the amorphous phase (Am_1 and Am_2). In addition, some MS were obtained by applying a magnetic field of 0.2 T perpendicularly to the gamma-ray direction (in samples Ge10 and Ge13.5) in order to verify the hyperfine parameters under different experimental configurations.

Saturation magnetization (M_s) was measured in a Physical Property Measurement System (PPMS) and at a maximum applied field of 5 T. Coercivity was obtained from the hysteresis loops measured on open strips using a quasi-static fluxmetric method by applying an axial field on the sample and collecting the induced signal in a secondary air-compensated pick-up coil. All experiments were performed at room temperature.

3. Results

Figs. 1(a)–(d) show, as an example, the MS of samples Ge15.5*, Ge13.5 and Ge0 and the fits performed on them. They clearly exhibit an increment in crystalline subspectra as the Ge content increases. Some results obtained from these fits are listed in Table 1: the relative area corresponding to Fe in the amorphous phase (n^{am}), the area ratio between lines 2 and 3 for crystalline sites ($D23$), and the hyperfine magnetic field of Am_1 sextext (Bhf^{am}). The at% of Si+Ge in nanograins was calculated via the relative resonant absorption area of sextets $S1$–$S4$, $S5$ and $S6$ after careful fits [11,20]. These data were systematically compared after each fit with the area of an ideal DO_3 non-stoichiometric spectrum (at different chemical composition) in order to minimize the errors in the fitting. Then, the best combination of MS fit and DO_3 area fit was adopted. The error in the determination of the chemical composition found during these approaches was about $\pm$0.3%. From XRD results, we obtained the nanocrystalline grain diameter (D) employing the Scherrer formula [21] and the lattice parameter (a) of the DO_3 structure. These data are also included in Table 1. MS results show that the n^{am} and Bhf^{am} decrease as the %Ge increases in the master alloy. The parameter $D23$ decreases with the %Ge content from $D23 \approx 3$ to $D23$=1.6, which indicates that the preferential alignment of the local magnetic moments changes from near the ribbon surface plane to a more perpendicular one (passing through a random distribution at $D23$=2). Also, the solute (Si+Ge) content in nanograins seems to decrease with the addition of Ge and its lattice parameter (obtained by XRD) increases in agreement with the larger atomic radius size of Ge. Comparing the MS results of the samples submitted to a magnetic field of B_{app}=0.2 T and with those B_{app}=0 T there was a difference of less than 2.5% in the calculation value of the amorphous resonant area (n^{am}). This shows that the fits are of good quality. The MS of sample Ge13.5 with B_{app}=0.2 T is shown in Fig. 1(b) and some hyperfine parameters are listed in Table 1 together with those of sample Ge10 obtained in the same experimental configuration.

4. Discussion

4.1. Nanocrystal chemical composition

Usually, chemical composition of α-Fe(Si) nanocrystals in FINEMET-type alloys is determined either with the value of bcc lattice parameter obtained by XRD or by employing the MS technique. However, in the case of three component α-Fe(Si,Ge) nanocrystals, it is not possible to determine chemical composition from XRD results since the lattice parameter decreases with Si content and increases with Ge content. Similarly, the MS resonant areas of an α-Fe(Si,Ge) DO_3 structure only give us information about the total content of Si+Ge solutes. In order to solve this problem, we combined data obtained from both XRD and MS techniques and computed the content of Ge and Si in nanograins as follows: Starting from lattice parameter data (a) available in the literature for α-Fe(Si) and α-Fe(Ge) bicomponent alloys and based on Vergard's law [22] we established a linear relationship

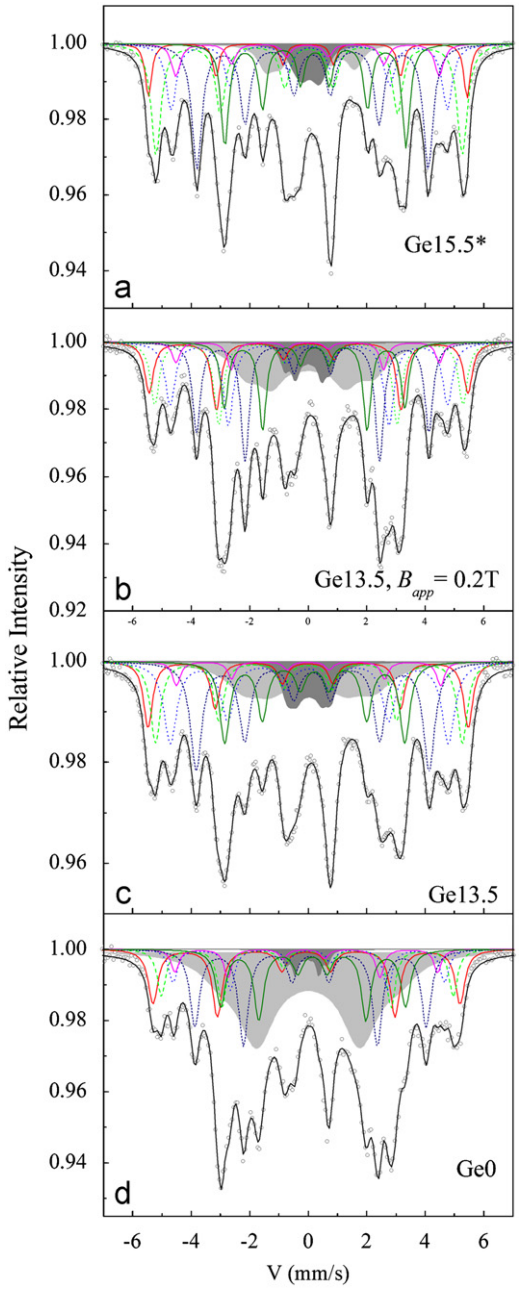

Fig. 1. Mössbauer spectrum of samples: (a) Ge15.5*, (b, c) Ge13.5 and (d) Ge0: the dots and the continuous line represent, respectively, the spectrum data and the fitting performed on it. The six subspectra of the crystalline phase, associated with different Fe sites are shown in different line styles and the residual amorphous phase is marked by the two shadowed subspectra. Fig. 1(b) corresponds to a B_{app}=0.2 T experimental configuration.

between the lattice parameter and the solute concentration (x), $a(x)$, for an α-$Fe_{100-y}(Si_{1-x}Ge_x)_y$ cell, where $0 \le x \le 1$. We fixed y, the total solute content, at various values between 18.2 and 22.2 according to the total percentage of solutes content in alloys obtained by MS analysis (see data in Table 1). For example, in the case of sample Ge8 we have $Fe_{81.7}(Si_{1-x}Ge_x)_{18.3}$ (where y=18.3) and data $a(0)$=5.67035Å (for $Fe_{81.8}Si_{18.2}$) [23] and $a(1)$=5.768Å (for $Fe_{81.8}Ge_{18.2}$) [11]. The resulting linear relationship was (in Å):

$$a_{y=18.2}(x) = 5.67035 + 0.00537xy \quad (1)$$

Using a and y data (from XRD and MS techniques, respectively) of sample Ge8, we can obtained the value of x and then xy that is the %Ge content in nanocrystals (at%). The same procedure was employed for y=22.2 (sample Ge6*). In this case, we used the lattice parameters of $Fe_{75}Si_{25}$ (a=5.641Å [23]) and $Fe_{75}Ge_{25}$ (a=5.796Å [24]) and created curves with equal content of solutes y between the known values of y=18.2 and 25. Fig. 2(a) gives the %Ge in the master alloy vs. the lattice parameter, and Fig. 2(b) exemplifies the graphic procedure for obtaining the % Ge in nanocrystals. Table 2 lists the chemical composition of nanograins.

With chemical composition and a data it is possible to determine the mass density of nanocrystals that will be useful in forthcoming analysis in Section 4.4. These results are also included in Table 2 and agree with literature data for mass density of bcc Fe_3Ge, $\delta \sim 8.14$ g/cm^3[24].

4.2. Phase volume fractions

In order to obtain the amorphous matrix composition, we first determined the crystalline and amorphous volume fractions using the MS technique. From the MS fittings, one can obtain the relative amount of Fe contained in crystalline and amorphous phases, considering the same recoilless factors for both of them. Traditional methods assume that these areas are proportional to the volume of both phases. However, we must take into account that the percentage amount of Fe contained in the amorphous phase may be quite different from that of the nanocrystalline one; this could induce errors that in the cases of high crystalline fractions and/or high Fe content in nanocrystals could be relevant. To obtain more accurate results, we introduce other method for determining the volume phases of a nanocrystalline alloy and, therefore, the chemical composition of the amorphous phase. It is based on a simple volume balance method and we do not take into account either density or recoilless factor differences between amorphous and nanocrystalline phases. These considerations allow the calculation of the relative amount of Fe contained in the nanocrystalline (n^{cr}) and amorphous (n^{am}) phases in the following way:

$$n^{cr} = \frac{Fe^{cr}}{Fe^{cr} + Fe^{am}} \quad (2)$$

and

$$n^{am} = \frac{Fe^{am}}{Fe^{cr} + Fe^{am}} \quad (3)$$

where Fe^{cr} and Fe^{am} are proportional to the atomic content of Fe in crystalline and amorphous phases, respectively. In the appendix, we demonstrate that, disregarding density differences between crystals and matrix, Eq. (2), for example, can be rewritten as

$$n^{cr} = \frac{m_{Fe}^{cr} v^{cr}}{m_{Fe}^{aq}} \quad (4)$$

where v^{cr} is the volume fraction of the crystalline phase, m_{Fe}^{cr} its iron mass fraction (wt%) and m_{Fe}^{aq} is the mass fraction of iron in the as-quenched alloy. The mass fractions m_{Fe}^{cr} and m_{Fe}^{aq} are known data that can be obtained from the atomic composition of the nanocrystals (see Section 4.1) and the nominal composition of the alloys, respectively. Thus, the volume fraction v^{cr} can be easily determined. The assumption of equal densities of the phases is well established for a FINEMET alloy since its density in the nanocrystallized state (i.e., nanocrystals plus amorphous matrix) is 7.35 g/cm^3 and the calculated density of a $Fe_{81.5}Si_{18.5}$ crystalline alloy is 7.395 g/cm^3 (using lattice parameter data from Ref. [23]).

Fig. 3 presents the crystalline volume fraction (v^{cr}) of series A samples as a function of the Ge content of the master alloy. It is possible to see that for identical annealing conditions the Ge substitution for Si causes the v^{cr} increase. Table 2 collects these

Table 1
Nominal composition of samples and results obtained from Mössbauer spectroscopy and X-ray diffraction: relative area of Fe in amorphous phase (n^{am}); area absorption ratio between lines 2 and 3 (or 5 and 4) for crystalline sites ($D23$); hyperfine magnetic field of Am_1 (amorphous) sextet (Bhf^{am}); at% content of Si+Ge in nanograins (y); lattice parameter of nanograins (a); grain diameter (D); at% content of Ge in nanograins (Ge).

Serie	Sample	Master alloy	n^{am} (%)	$D23$	Bhf^{am} (T)	y % (Si+Ge)	a (Å)	D (nm)	Ge (at%)
A	Ge0	$Fe_{73.5}Si_{13.5}B_9Nb_3Cu_1$	39.0	3.1	18.7	19.0	5.667	12	0
A	Ge7	$Fe_{73.5}Si_{6.5}Ge_7B_9Nb_3Cu_1$	32.0	3.3	14.7	18.6	5.721	12	9.4
A	Ge8	$Fe_{73.5}Si_{5.5}Ge_8B_9Nb_3Cu_1$	28.5	2.9	14.1	18.3	5.727	13	10.6
A	Ge10	$Fe_{73.5}Si_{3.5}Ge_{10}B_9Nb_3Cu_1$	27.1	2.8	14.0	18.5	5.744	13	13.7
	Ge10	with B_{app}= 0.2T	24.8	4	13.4	18.3	–	–	–
A	Ge13.5	$Fe_{73.5}Ge_{13.5}B_9Nb_3Cu_1$	21.2	2.1	13.9	18.2	5.768	13	18.2
	Ge13.5	with B_{app}= 0.2T	22.5	4	13.6	17.9	–	–	–
–	Ge6*	$Fe_{71.5}Si_{9.5}Ge_6B_9Nb_3Cu_1$	33.0	3.2	14.1	22.2	5.706	14	9.25
–	Ge15.5*	$Fe_{73.5}Ge_{15.5}Nb_3B_7Cu_1$	12.3	1.6	9.4	18.6	5.769	15	18.6

Errors in D= ± 2 nm, y= ± 0.3%, a= ± 0.002Å, n^{am}= ± 2.5%, $D23$= ± 0.2 and Bhf^{am}= ± 0.5 T.

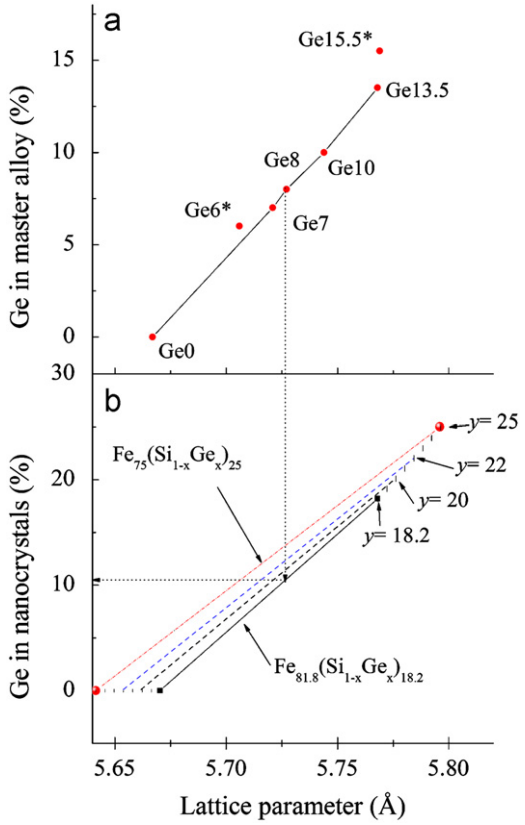

Fig. 2. (a) Ge content (at%) in the master alloy vs. the lattice parameter and (b) procedure for obtaining the Ge in nanocrystals. Straight lines in graph, (b) correspond to curves obtained from Eq. (1) where solute content Si+Ge=(y) is identical.

Table 2
Chemical composition for nanocrystals (obtained from Eq. (1)) and amorphous matrix (Eq. (5)), and crystalline volume fraction (v^{cr}) (Eq. (4)).

Sample	δ (g/cm^3)	v^{cr} (%)	Nanocrystals			Amorphous matrix						
			Fe	Si	Ge	Fe	Si	Ge	Cu	Nb	B	Si+Ge
Ge0	7.38	56.9	81.0	19.0	0	64.2	6.7	0	2.2	6.7	20.2	6.7
Ge7	7.79	64.4	81.4	9.2	9.4	60.9	2.2	3.2	2.6	7.8	23.3	5.4
Ge8	7.85	67.6	81.7	7.7	10.6	58.7	1.5	3.3	2.8	8.4	25.2	4.8
Ge10	7.97	69.6	81.5	4.8	13.7	58.1	1.0	2.9	2.9	8.8	26.3	3.9
Ge13.5	8.16	75.5	81.8	0	18.2	53.4	0	2.1	3.4	10.3	30.8	2.1
Ge6*	8.27	64.5	77.8	12.9	9.3	61.4	4.0	0.8	2.6	7.8	23.4	4.8
G315.5*	8.16	82.7	81.4	0	18.6	43.4	0	3.7	4.8	14.4	33.6	3.7

The mass density (δ) was calculated taking into account lattice parameter data.

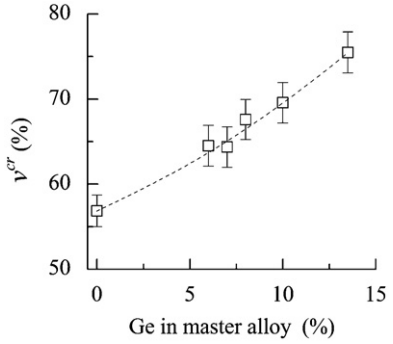

Fig. 3. Crystalline volume fraction v^{cr} of samples of series A as function of the Ge content of the master alloy, obtained from Eq. (4).

results and allows for further analysis: A slight impoverishment of solutes (Si+Ge) seems to be present in the crystalline phase as v^{cr} increases. The exception is sample Ge6*, which has a lower Fe content in the master alloy; here an important increment in solute content is observed. This effect was already observed when Fe was substituted by Si [9].

Considering an error of ± 2.5% in the calculus of n^{cr} (or n^{am}, as previously stated) the error in the v^{cr} calculus will be less than ± 2.5% because $m_{Fe}^{cr} > m_{Fe}^{aq}$ (see Eq. (4)) in our nanocrystallized alloys.

4.3. Amorphous matrix composition

Once we have obtained the volume fraction of the phases, it is possible to calculate the chemical composition of the amorphous remnant matrix in nanocrystallized samples employing the mass balance formula:

$$m_i^{alloy} = m_i^{cr} v^{cr} + m_i^{am}(1 - v^{cr}) \quad (5)$$

where i refers to the different elements in the alloy. This analysis does not take into account that Cu is clustered in very rich fcc phase [25] and instead it is considered part of the amorphous matrix without detriment of the conclusions. Table 2 also shows the results of the chemical composition obtained for the intergranular amorphous matrix. The increment in v^{cr} causes a reduction in Fe and Si+Ge content in the amorphous phase and an increment in Nb and B that can deteriorate the soft magnetic properties of the material. This is more evident in sample Ge15.5*. For sample Ge6*, the matrix composition remains very similar to that of Ge7 in spite of its higher content of Si+Ge in the master alloy. It is worth noting that one can obtain near the same v^{cr} and

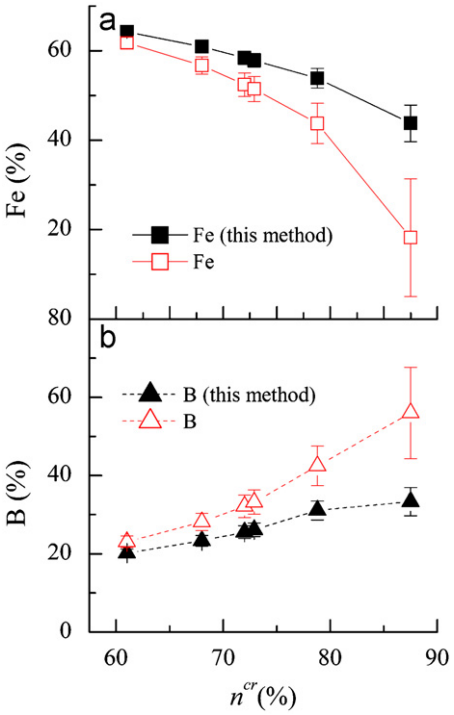

Fig. 4. (a) Fe and (b) B content of the amorphous matrix obtained by this method (full symbols) and the traditional one (open symbols).

a comparable chemical composition in the amorphous phase, with two different solute contents in the master alloy (i.e., Si+Ge equals to 13.5% in Ge7 and 15.5% in Ge6*). The error in the calculation of the chemical composition of the matrix is smaller compared with the traditional method because of error reduction when obtaining v^{cr}. As an example, Fig. 4 compares the Fe and B content of the amorphous matrix obtained by this method and by the traditional one. The error bars resulted from considering the error of $\pm 2.5\%$ in the calculus of n^{cr}. It can be observed that the greater the crystalline fraction, the greater the error in the chemical composition of the matrix. Under this condition, we have a maximum error of $\pm 4.2\%$ and $\pm 3.6\%$ that corresponds to the Fe and to the B in the amorphous matrix, respectively, at n^{cr}=87.7% (sample Ge15.5*). For the rest of the elements dissolved into the matrix, the error is about $\pm 1\%$.

Figs. 5(a)–(c) show the at% in the amorphous matrix of Si+Ge (a), Nb and B (b) and Fe (c) in function of v^{cr} for each sample. Some other sample data found in the literature for FINEMET-like alloys were also analyzed and included in these graphs [20,26]. Dashed lines show the theoretical evolution with respect to v^{cr} in the case of a typical $Fe_{73.5}Si_{13.5}Nb_3B_9Cu_1$ nanocrystalline alloy with 19 at% Si in nanocrystals, by using Eq. (5). In Fig. 5(a), the theoretical curve for 18 at% Si in nanocrystals is also plotted for comparison. The curves show that at about v^{cr}=75% the content of Si in the amorphous matrix will be negative, thus it is not possible to obtain a 19% Si in nanocrystals with a crystalline fraction of v^{cr}=75%; this forces a reduction of Si content (for example to ~18%). This is why sample Ge15.5* with the highest Si+Ge content of all the series has only 18.2% Ge in nanograins due to its high v^{cr} (82.7%). The inset in Fig. 5(a) shows how samples in the same series with equal Si+Ge content in master alloy (i.e., 13.5%) reduce its content in nanograins as v^{cr} increases. A high crystalline fraction will also make the B and Nb content increase rapidly (Fig. 5b) as well as impoverish the Fe content in the matrix (Fig. 5c), which can affect the soft magnetic properties of the entire material.

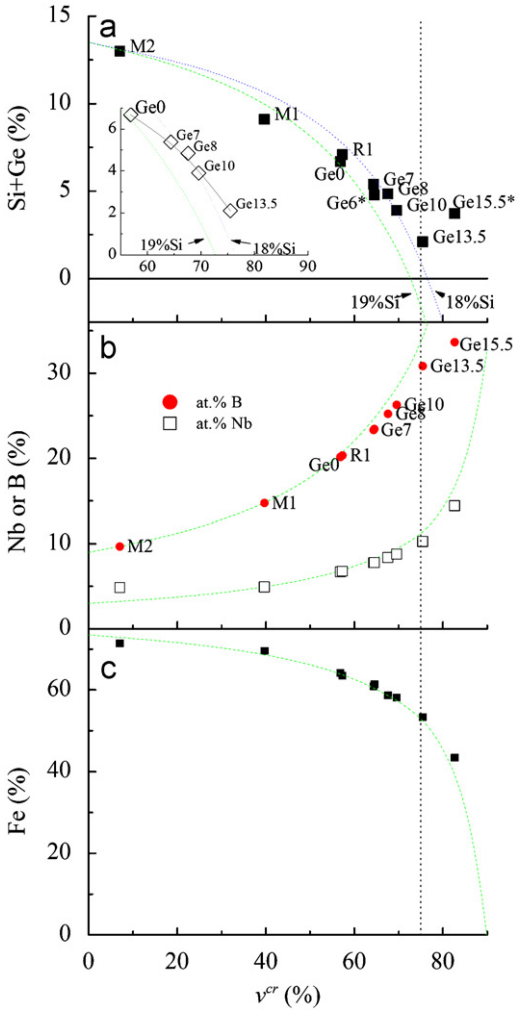

Fig. 5. Chemical composition (at%) variation of the amorphous matrix as a function of v^{cr}: (a) Si+Ge, (b) Nb and B and (c) Fe. M1 and M2 correspond to $Fe_{73.5-x}Si_{13.5}B_9Nb_xCu_1$ with x=3 and 4.5, respectively [26], and R1 corresponds to $Fe_{73.5}Si_{13.5}B_9Nb_3Cu_1$[20].

4.4. Saturation magnetization and exchange stiffness

Saturation magnetizations (M_s), in emu/g, of most of the samples have already been published [12–14]. Using density data from Section 4.1, we obtain an approximate value of M_s in Tesla. Results are listed in Table 3. In previous papers [12,13], we used a lineal model to calculate the saturation magnetization of α-Fe(Si,Ge) DO_3 crystals (M_s^{cr}). Using the same procedure, the M_s^{cr} is calculated and, given the total saturation magnetization of the sample (M_s^{tot}) that of the amorphous matrix (M_s^{am}) can be analyzed using the simplification $M_s^{tot}=M_s^{cr}\cdot v^{cr}+M_s^{am}(1-v^{cr})$.

Fig. 6 shows the experimental M_s^{tot} values and the calculated M_s^{cr} and M_s^{am} values as a function of v^{cr}. In Ref. [12], we succeeded in obtaining an amorphous ribbon of composition $Fe_{58}Si_{0.5}Ge_{3.5}Cu_3Nb_9B_{26}$ named AM-Ge10 (emulating the amorphous matrix of nanocrystalline sample Ge10: $Fe_{58.1}Si_{1.0}Ge_{3.0}Cu_3Nb_{8.7}B_{26.2}$). The M_s of sample AM-Ge10 was experimentally measured given a value of 116.66 emu/g that corresponds to M_s=1.17 T (using density data of Ge10 crystals). This value of amorphous matrix is in good agreement with the ones of the present work (see Table 3). The inset of Fig. 6 shows the behavior of M_s^{am} with iron in amorphous matrix. The M_s^{am} value calculated for sample Ge15.5* is too high (95 emu/g or

Table 3
Saturation magnetization (M_s), magnetic moment per Fe atom (μB/at), magnetostriction constant (λ_s), exchange stiffness constants (A), random magnetocrystalline anisotropy ($\langle K_1 \rangle$) obtained from Eq. (9), intergranular distance (Λ), for crystalline (cr), and amorphous (am) phases and for nanocrystalline material.

Sample	Crystalline phase			Amorphous matrix			Nanocrystalline material			
	M_s^{cr} (T)	μB/at	λ_s^{cr} (10^{-6})	M_s^{am} (T)	A_{am} (10^{-12})	μB/at	$\langle K_1 \rangle$ (J/m^3)	M_s^{tot} (T)	A_{cr}/A_{am}	Λ (Å)
Ge0	1.39	1.68	−7(2)	1.23	7.6(3)	1.76	4(2)	1.33(1)	0.78	25(1)
Ge7	1.45	1.79	−6(2)	1.22	7.4(3)	1.78	6(3)	1.37(1)	0.71	19(1)
Ge8	1.46	1.81	−5(3)	0.94	6.5(7)	1.70	12(5)	1.36(2)	0.61	18(1)
Ge10	1.48	1.84	−15(3)	1.10	6.0(4)	1.61	12(5)	1.36(1)	0.55	16(1)
Ge13.5	1.50	1.88	−23(3)	0.99	4.9(4)	1.51	16(6)	1.37(1)	0.44	12(1)
Ge6*	1.38	1.64	−6(2)	1.22	7.4(4)	1.62	1(2)	1.32(1)	0.78	21(1)
Ge15.5*	1.48	1.88	−33(3)	0.98	4(1)	1.84	38(8)	1.40(2)	0.43	9(1)

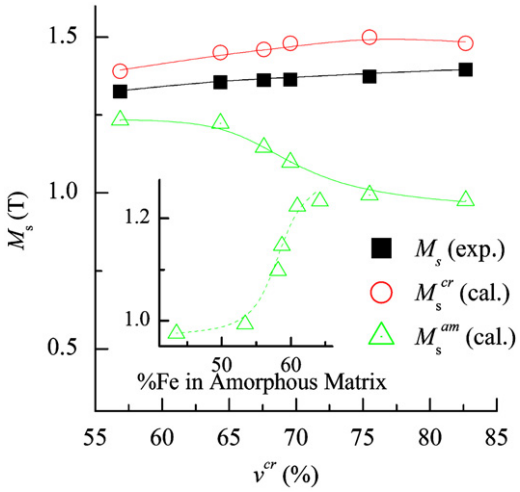

Fig. 6. Saturation magnetization of nanocrystallized samples vs. v^{cr} for the sample experimentally measured (M_s^{tot}) (full squares), and the ones calculated for the crystalline phase (M_s^{cr}) (open circles) and the amorphous phase (M_s^{am}) (open triangles). Inset shows M_s^{am} as function of the Fe content in amorphous matrix.

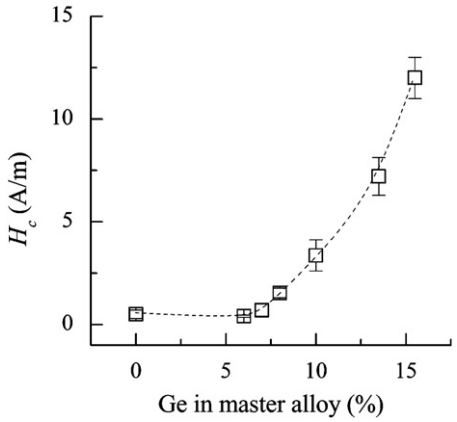

Fig. 7. Magnetic coercive field (H_c) evolution with Ge content in master alloy of nanocrystallized samples.

0.97 T) given that the amount of Fe in remnant amorphous matrix is calculated to be ∼43%. This could be a consequence of the exchange field penetration of nanocrystals into the amorphous matrix. In fact, the magnetic moment per Fe atom for the amorphous matrix of Ge15.5* (M_s^{am}=95 emu/g) is about 1.84 μB/per Fe atom, the largest of all the series (summarized in Table 3), while the one for its nanocrystals is 1.875 .μB/at. It is well established [27] that the penetration of the exchange field can enhance the Curie temperature up to 125 °C with an intergranular distance $\Lambda = D(1/v^{cr})^{1/3} - D = 40$ Å. The intergranular distances calculated in this work are considerably smaller than the ones of Ref. [27] and sample Ge15.5* has the smallest intergranular distance of all the samples presented in this work. A similar experience was already presented by Škorvánek et al. [28] in a $Fe_{80.5}Nb_7B_{12.5}$ nanocrystallized alloy (26% nanocrystalline phase). They observed an increment in the magnetization of the intergranular amorphous matrix ($\Delta M_s^{am} \sim 20$ emu/g) when comparing with the experimental value of an identical matrix composition full amorphous alloy ($M_s^{am} \sim 53$ emu/g, at room temperature). They concluded that this peculiar behavior is a consequence both of a strong chemical heterogeneity of the intergranular amorphous phase (i.e., different Fe-rich zones in the matrix) not presents in the non-nanocrystallized amorphous alloy, and of the contribution of penetrating fields. In view of the difference in crystalline volume fraction (as well as in the intergranular distance) and in the amorphous matrix chemical composition (note the poor Fe content of sample Ge15.5* matrix) between Ref. [28] and Ge15.5* alloys, it is reasonable to consider that in our case, penetrating fields are the main causes of the M_s^{am} increment.

At this point, it is possible to stipulate the value of the exchange stiffness constant of nanocrystals A_{cr} and of the amorphous matrix A_{am} that will be useful in later calculations. The exchange stiffness is known to be proportional to M_s^2/a. Knowing the exchange stiffness of pure Fe, $A_{Fe} = 2 \times 10^{-11}$ J/m [29], and its magnetic saturation magnetization, M_s=2.0 T, we can correlate it M_s^{cr} and M_s^{am} of α-Fe(Si,Ge) crystals and amorphous matrix, respectively. The A_{cr} and A_{cr}/A_{am} values obtained are shown in Table 3 (lattice parameter (a) is also employed in the calculations but has little relevance).

4.5. Magnetic hardening

Fig. 7 shows the behavior of the coercive magnetic field (H_c) with Ge content of the master alloy for all nanocrystallized samples analyzed in this work. We can see an increase in the H_c with increasing Ge content starting at about 8% Ge. We now explain this fact. It is known that

$$H_c = p_c \langle K \rangle / M_s \tag{6}$$

where p_c is a constant determined to be equal to 0.2 for FINEMET-like alloys [6]. Considering that M_s varies slightly in our samples (see Fig. 6), we must investigate the origin of magnetic hardening in the effective anisotropy constant $\langle K \rangle$. Using Eq. (6), we obtain the values of $\langle K \rangle$ and plot them against v^{cr} in Fig. 8.

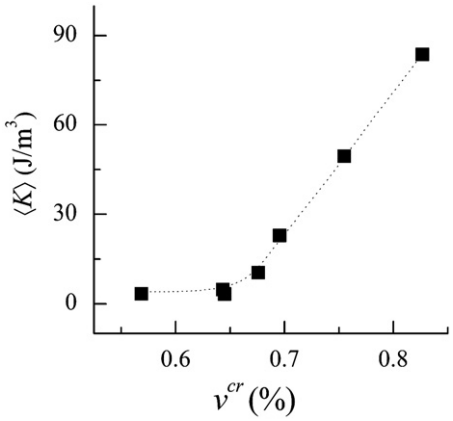

Fig. 8. Dependence of the effective anisotropy constant $\langle K\rangle$ on v^{cr} of nanocrystallized samples.

The effective anisotropy constant $\langle K\rangle$ is determined by various magnetic anisotropies; it can be established that [30]:

$$\langle K\rangle = \sqrt{\langle K_1\rangle^2 + \sum_i Ku_i^2} \tag{7}$$

where $\langle K_1\rangle$ is the random magnetocrystalline anisotropy and Ku_i are uniaxial anisotropies (such us magneto-elastic and field-induced anisotropies). We take into account two cases in the study of these anisotropies.

On the one hand, the random magnetocrystalline anisotropy $\langle K_1\rangle$ can be evaluated by different models, wherein the local magnetic anisotropy of the amorphous remnant phase is neglected because of its very low value compared with that of the crystalline phase. Two models are considered:

(a) Herzer's model [6], the simplest one, that takes into account the crystalline volume fraction, v^{cr}:

$$aK_1\tilde{n} = v^{cr2}K_1^4D^6/A_{cr}^3 \tag{8}$$

(b) Suzuki's model [8] that takes into account also the exchange stiffness A_{am} of the intergranular amorphous phase:

$$\langle K_1\rangle = \frac{(A_{cr})^3}{L_0^6}(v^{cr})^4K_1D^6\left[\frac{1}{\sqrt{A_{cr}}} + \frac{(v^{cr})^{-1/3}-1}{\sqrt{A_{am}}}\right] \tag{9}$$

where the intrinsic exchange correlation length (L_0) is ~35 nm for α-Fe(Si) grains with 20% Si [6].

On the other hand, the only induced anisotropies acting in the sample are the magnetoelastic (Ku^{el}). So,

$$Ku = Ku^{el} = 3/2|\lambda_s \times \sigma_i| \tag{10}$$

where σ_i are internal stresses in the material. The magnetostriction constant of the whole material (λ_s) can be determined by [31]:

$$\lambda_s = v^{cr}\lambda_s^{cr} + (1-v^{cr})(\lambda_s^{am} + kv^{cr}) + 3v^{cr}\lambda_s^s/R \tag{11}$$

where λ_s^{cr} and λ_s^{am} are the magnetostriction constants of crystalline and amorphous phases, respectively, k is a parameter that takes into account the amorphous matrix magnetostriction evolution, λ_s^s is the magnetostriction constant of the interface surface–volume of the nanocrystals and R is the average radius of nanograins.

Magnetocrystalline anisotropy data for α-Fe(Si) with Si content greater than 14% is very scarce [32]. The anisotropy constant K_1 of the α-Fe(Si) solid solution monotonically decreases from 53 kJ/m^3 for pure iron to ~0 J/m^3 for 23.1% Si [33]; a value of K_1=8 kJ/m^3 was reported [6] for α-$Fe_{80}Si_{20}$. K_1 for α-Fe(Ge) is reported to have a very similar behavior as α-Fe(Si), in the range up to ~6% Ge [34]. Fig. 9 collects all these literature data.

No data could be found in the literature for higher Ge content either in the α-Fe(Ge) structure or in the α-Fe(Ge,Si) one. Thus, we will assume K_1=8 kJ/m^3 for all α-Fe_{100-x}(Si,Ge)$_x$ with $x \approx 19$ and K_1 near zero for x=22.

The behavior of $\langle K\rangle$ vs. v^{cr} shown in Fig. 8 was fitted using Eq. (7) where $\langle K_1\rangle$ was evaluated with both models in Eqs. (8) and (9) and Ku^{el} with Eqs. (10) and (11). An estimated internal stress value of σ_i=2 MPa was considered [9] when determining Ku^{el}. After several fitting assumptions of K_1 and λ_s^{cr} for the α-Fe(Si,Ge) grains and λ_s^{am} for the matrix, it was concluded that the principal factor causing the magnetic hardness in Ge-containing nanocrystalline alloys was a high negative magnetostriction occurring in the α-Fe(Si,Ge) nanocrystals. This conclusion is based on the following: (a) A much higher value of K_1=8 kJ/m^3 for the α-Fe_{81}(Si,Ge)$_{19}$ alloy is unlikely because of the trend observed in Fig. 9; in addition it does not match our fittings at all. (b) In a recent work, Wu et al. [35] determined the $\lambda_{s[1\,0\,0]}$ of α-Fe(Ge) crystals obtaining $\sim -85\times10^{-6}$ for 18% Ge that is about 10 times higher (in absolute value) than λ_s for the α-$Fe_{80}Si_{20}$. Our fitting results denote a λ_s^{cr} of around -30×10^{-6} for α-$Fe_{81.5}Ge_{18.5}$ (samples Ge13.5 and Ge15.5*).

The behavior of λ_s^{cr} with Ge content in the α-$Fe_{81.5}Si_{18.5-x}Ge_x$ was obtained from the fits and is shown in Fig. 10. To compute it, we assumed that the typical values for FINEMET are $\lambda_s=2.1\times10^{-6}$, $\lambda_s^{cr}=-7\times10^{-6}$ and $\lambda_s^{am}=22\times10^{-6}$[9,36], while the fitting values were $\lambda_s^s=6\times10^{-6}$ nm [31], and $k=-28\times10^{-6}$[36]. We can observe a plateau up to x=9.4 and then a decrease reaching a value of λ_s^{cr} $\sim30\times10^{-6}$ for a composition near α-$Fe_{81.5}Ge_{18.5}$ (samples Ge13.5 and Ge15.5*). The difference in λ_s^{cr} values between Ge13.5 and Ge15.5* observed in Fig. 10, can be explained by a slightly higher internal stress value perhaps due to the higher crystalline fraction that induces extra lattice mismatch (e.g., adopting σ_i=3 MPa instead of 2 MPa in Eq. (10) for fitting data of sample Ge15.5* we obtain the same $\lambda_s^{cr}=-23\times10^{-6}$ as for sample Ge13.5). This assumption can also explain the value of the peaks area ratio $D23$=1.6 in Mössbauer spectroscopy results for sample Ge15.5* (Table 1): although the stresses produced by the devitrification process are randomly oriented, its distribution will have a preference alignment perpendicular to the surface plane due to the ribbon shape of the sample.

To conclude, in a recent article, Sato Turtelli et al. [37] obtained a magnetostriction constant of -30×10^{-6} for a $Fe_{80}Ge_{20}$ polycrystalline alloy. This is very consistent with the results presented in this work.

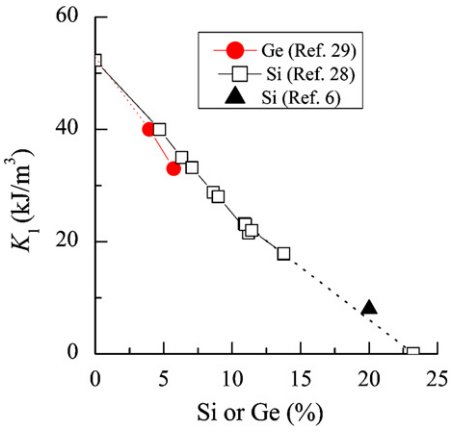

Fig. 9. Magnetocrystalline anisotropy constant (K_1) for α-Fe(Si) and α-Fe(Ge) solid solutions as a function of the Si or Ge content. Data obtained from Refs. [6,33,34].

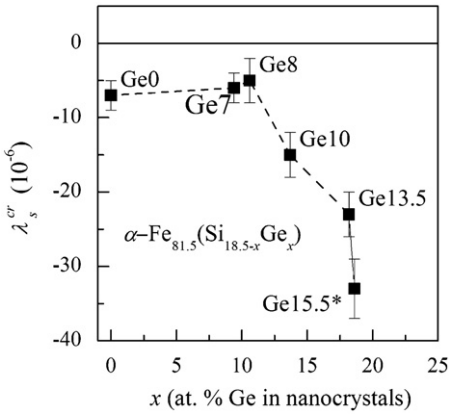

Fig. 10. Magnetostriction constant for the α-$Fe_{81.5}(Si,Ge)_{18.5}$ with different Si/Ge content obtained by fitting the behavior of $\langle K \rangle$ in Fig. 8 with Eqs. (7)–(10).

5. Conclusions

Chemical composition of α-Fe(Si,Ge) nanocrystals was calculated via a simple model using data from XDR and MS. In addition, a model to calculate the volume fractions of amorphous and crystalline phases on nanocrystallized samples, based in MS results, was introduced leading to more accurate data of v^{cr} and hence, of chemical composition of the amorphous matrix.

Structurally, the effect of the addition of Ge in the nanocrystallized $Fe_{73.5}Si_{13.5-x}Ge_x$ $B_9Nb_3Cu_1$ (FINEMET-like) alloy can be summarized as follows:

(a) In series A (with 13.5% (Ge+Si) in master alloys), the Ge substitution for Si causes an increase in the crystalline volume fraction as well as a reduction of Si+Ge in the amorphous matrix. In addition, there is a trend of solute (Si+Ge) impoverishment in the α-Fe(Si,Ge) nanograins that is in accord with the increment in v^{cr}.
(b) This latter behavior is also verified in sample Ge15.5* (with 15.5% Ge in master alloy), which has the highest v^{cr} of all studied alloys and 18.6%Ge in the α-Fe(Ge) nanograins while the matrix composition is enriched in Nb and B elements.
(c) For sample Ge6* (with 15.5% (Ge+Si) in master alloy) the v^{cr} and matrix composition is very similar to that of sample Ge7 but, instead, the solute content in nanograins increases due to a lower Fe content in master alloy.
(d) Finally, we present values of mass densities for the α-Fe(Si,Ge) crystals calculated using the composition and lattice parameters.

With respect to magnetic properties, the behavior of the M_s^{am} of the amorphous intergranular matrix with its Fe content seems to be strongly affected by the exchange field penetration regardless of the Fe content of the matrix. This is because a small intergranular distance is reached in presence of high v^{cr}. Another consequence is that the exchange stiffness constant for the nanograins and for amorphous phases (A_{cr} and A_{am}) is almost of the same order. The evaluation of Herzer and Suzuki's models shows that the magnetic hardening observed when increasing % Ge content could not be attributed to an increase in $\langle K_1 \rangle$, v^{cr}, or the ratio A_{cr}/A_{am} but principally to an important increment in the magnetostriction constant of the α-Fe(Si,Ge) nanocrystals, whose values were estimated.

Appendix

The relative number n^{cr} of Fe atoms in crystalline phase is obtained from the Mössbauer spectrometry results:

$$n^{cr} = \frac{Fe^{cr}}{Fe^{cr} + Fe^{am}} \tag{A.1}$$

where Fe^{cr} and Fe^{am} represent the total number of Fe atoms in nanocrystalline and amorphous phases, respectively.

Multiplying numerator and denominator of Eq. (A.1) by the atomic weight of Fe we obtain the same relation expressed in mass:

$$n^{cr} = \frac{M_{Fe}^{cr}}{M_{Fe}^{cr} + M_{Fe}^{am}} \tag{A.2}$$

Now we can write

$$M_{Fe}^{cr} = M_{Fe}^{cr}\left(\sum_i M_i^{cr} / \sum_i M_i^{cr}\right) \tag{A.3}$$

and

$$M_{Fe}^{am} = M_{Fe}^{am}\left(\sum_i M_i^{am} / \sum_i M_i^{am}\right) \tag{A.4}$$

where M_i^{cr} (or M_i^{am}) represent the mass of the i element in the nanocrystalline (or amorphous) phase. On the other hand, we can divide numerator and denominator by the total mass of the alloy, represented in the as-quenched state: $\Sigma_i M_i^{aq}$. Then, Eq. (A.2) is equal to

$$n^{cr} = \frac{M_{Fe}^{cr}\left(\sum_i M_i^{cr} / \sum_i M_i^{cr}\right) / \sum_i M_i^{aq}}{M_{Fe}^{cr}\left(\sum_i M_i^{cr} / \sum_i M_i^{cr}\right) / \sum_i M_i^{aq} + M_{Fe}^{am}\left(\sum_i M_i^{am} / \sum_i M_i^{am}\right) / \sum_i M_i^{aq}} \tag{A.5}$$

The ratios $\sum_i M_i^{cr} / \sum_i M_i^{aq}$ and $\sum_i M_i^{am} / \sum_i M_i^{aq}$—assuming the same densities between amorphous and nanocrystalline phases—are equal to the volume ratio of nanocrystalline and amorphous phases, v^{cr} and v^{am}, respectively. Ratios $M_{Fe}^{cr} / \sum_i M_i^{cr}$ and $M_{Fe}^{am} / \sum_i M_i^{am}$ are the mass fraction of Fe in each phase, m_{cr}^{Fe} and m_{am}^{Fe}.

Then, Eq. (A.5) can be rewritten as

$$n^{cr} = \frac{m_{Fe}^{cr} v^{cr}}{m_{Fe}^{cr} v^{cr} + m_{Fe}^{am} v^{am}} = \frac{m_{Fe}^{cr} v^{cr}}{m_{Fe}^{as}} \tag{A.6}$$

References

[1] Y. Yosizawa, S. Oguma, K. Yamauchi, J. Appl. Phys. 64 (1988) 6044.
[2] R. Alben, J.J. Backer, M.C. Chi, J. Appl. Phys. 49 (1978) 1653.
[3] G. Herzer, Mater. Sci. Eng. A 133 (1991) 1.
[4] A. Hernando, I. Navarro, in: G.C. Hadjipanayis, R.W. Siegel (Eds.), Nanophase Materials, Kluwer Academic Publishers, Netherlands, 1994, p. 703.
[5] G. Herzer, IEEE Trans. Magn. 25 (1989) 3327.
[6] G. Herzer, Scr. Metall. Mater. 33 (1995) 1741.
[7] A. Hernando, M. Vázquez, T. Kulik, C. Prados, Phys. Rev. B 51 (1995) 3581.
[8] K. Suzuki, J.M. Cadogan, Phys. Rev. B 58 (1998) 2730.
[9] G. Herzer, in: 1997th edition, in: K.H.J. Buschow (Ed.), Handbook of Magnetic Materials, vol. 10, Elsevier Science B.V., 1997, p. 415 (Chapter 3).
[10] M.E. McHenry, M.A. Willard, D.E. Laughlin, Prog. Mater. Sci. 44 (1999) 291.
[11] J. Moya, V.J. Cremaschi, H.R.M. Sirkin, Physica B 389 (2007) 159.
[12] D. Muraca, J. Moya, V.J. Cremaschi, H.R.M. Sirkin, Physica B 398 (2007) 325.
[13] D. Muraca, V.J. Cremaschi, J. Moya, H.R.M. Sirkin, J. Magn. Magn. Mater. 320 (2008) 810.
[14] D. Muraca, V.J. Cremaschi, J. Moya, H.R.M. Sirkin, J. Magn. Magn. Mater. 320 (2008) 1639.
[15] V.J. Cremaschi, G. Sánchez, H.R.M. Sirkin, Physica B 354 (2004) 213.
[16] J.M. Borrego, C.F. Conde, A. Conde, J.M. GrenècheJ. Phys.: Condens. Matter 14 (2002) 883–893.
[17] J.M. Cadogan, D.H. Ryan, in: D.R. Vij (Ed.), Handbook of Applied Solid State Spectroscopy, Springer Science+Business Media, LLC, 2006, p. 212 (Chapter 5).
[18] J.M. Borrego, A. Conde, V.A. Peña-Rodríguez, J.M. Grenèche, Hyp. Interact. 131 (2000) 67.
[19] J.M. Grenèche, Hyp. Interact. 110 (1997) 81.
[20] G. Rixecker, P. Schaaf, U. Gonser, J. Phys.: Condens. Matter 4 (1992) 10295.
[21] H.P. Klug, L.E. Alexander, in: X-ray Diffraction Procedure, 1954th ed., John Wiley & Sons Inc., New York, 1954, p. 492 (Chapter 9).

[22] L. Vegard, Z. Kristallogr. 67 (1928) 239.
[23] R.M. Bozorth, in: Ferromagnetism, 6th ed., D. Van Nostrand Company, INC, Princeton, New Jersey, 1961, p. 74 (Chapter 4).
[24] Y.S. Kwon, K.B. Gerasimov, O.I. Lomovsky, S.V. Pavlov, J. Alloys Compd. 353 (2003) 194.
[25] K. Hono, in: Y. Liu, D.J. Sellmyer, D. Shindo (Eds.), Handbook of Advanced Magnetic Materials, vol. 2, Springer, New York, 2006.
[26] M. Miglierini, J. Phys.: Condens. Matter 6 (1994) 1431.
[27] A. Hernando, I. Navarro, P. Gorría, Phys. Rev. B 51 (1995) 3281.
[28] I. Škorvánek, J. Kováč, J.M. Grenèche, J. Phys.: Condens. Matter 12 (2000) 9085.
[29] R.A. McCurrie, in: Ferromagnetic Materials, Structure and Properties, 1994th ed., Academic Press INC, San Diego CA, USA, 1994, p. 14 (Chapter 1).
[30] K. Suzuki, G. Herzer, J.M. Cadogan, J. Magn. Magn. Mater. 177–181 (1998) 949.
[31] A. Ślawska-Waniewska, H.K. Lachowicz, Scr. Mater. 48 (2003) 889.
[32] L.K. Varga, F. Mazaleyrat, J. Kovac, J.M. Greneche, J. Phys.: Condens. Matter 14 (2000) 1985.
[33] L.P. Tarasov, Phys. Rev. 56 (1939) 1231.
[34] R.C. Hall, J. Appl. Phys. 31 (1960) 1037.
[35] D. Wu, Q. Xing, R.W. McCallum, T.A. Lograsso, J. Appl. Phys. 103 (2008) 07B307.
[36] T. Szumiata, M. Gawroński, B. Górka, K. Brzózka, J.S. Blázquez-Gámez, T. Kulik, R. Żuberek, A. Ślawska-Waniewska, Nukleonika 48 (2003) S85.
[37] R. Sato Turtelli, C. Bormio Nunesa, L.C. Teixeira, R. Grössinger, P.A. Suzuki, C. Barbatti, J. Alloys Compd. 471 (2009) 52.
[38] R.A. Brand, Normos Program, Internal Report, Angewandte Physik, Universität Duisburg, 1987.